Surface plasmon microscopic sensing with beam profile modulation

Bei Zhang, Suejit Pechprasarn, and Michael G. Somekh*

Institute of Imaging and Optical Science (IBIOS), University of Nottingham, Nottingham NG7 2RD, UK
mike.somekh@nottingham.ac.uk

Abstract: Surface Plasmon microscopy enables measurement of local refractive index on a far finer scale than prism based systems. An interferometric or confocal system gives the so-called *V(z)* curve when the sample is scanned axially, which gives a measure of the surface plasmon propagation velocity. We show how a phase spatial light modulator (i) performs the necessary pupil function apodization (ii) imposes an angular varying phase shift that effectively changes sample defocus without any mechanical movement and (iii) changes the relative phase of the surface plasmon and reference beam to provide signal enhancement not possible with previous configurations.

OCIS codes: (180.0180) Microscopy; (110.0110) Imaging systems; (060.4080) Modulation; (120.0120) Instrumentation, measurement, and metrology.

References and links

1. H. Kano and W. Knoll, "Locally excited surface-plasmon-polaritons for thickness measurement of LBK films," Opt. Commun. **153**(4-6), 235–239 (1998).
2. M. G. Somekh, S. G. Liu, T. S. Velinov, and C. W. See, "High-resolution scanning surface-plasmon microscopy," Appl. Opt. **39**(34), 6279–6287 (2000).
3. M. G. Somekh, S. G. Liu, T. S. Velinov, and C. W. See, "Optical *V(z)* for high-resolution 2pi surface plasmon microscopy," Opt. Lett. **25**(11), 823–825 (2000).
4. M. G. Somekh, G. Stabler, S. Liu, J. Zhang, and C. W. See, "Wide-field high-resolution surface-plasmon interference microscopy," Opt. Lett. **34**(20), 3110–3112 (2009).
5. B. Zhang, S. Pechprasarn, J. Zhang, and M. G. Somekh, "Confocal surface plasmon microscopy with pupil function engineering," Opt. Express **20**(7), 7388–7397 (2012).
6. L. Berguiga, S. Zhang, F. Argoul, and J. Elezgaray, "High-resolution surface-plasmon imaging in air and in water: *V(z)* curve and operating conditions," Opt. Lett. **32**(5), 509–511 (2007).
7. S. Pechprasarn and M. G. Somekh, "Surface plasmon microscopy: resolution, sensitivity and crosstalk," J. Microsc. **246**(3), 287–297 (2012).
8. M. M. A. Jamil, M. C. T. Denyer, M. Youseffi, S. T. Britland, S. Liu, C. W. See, M. G. Somekh, and J. Zhang, "Imaging of the cell surface interface using objective coupled widefield surface plasmon microscopy," J. Struct. Biol. **164**(1), 75–80 (2008).
9. L. Berguiga, T. Roland, K. Monier, J. Elezgaray, and F. Argoul, "Amplitude and phase images of cellular structures with a scanning surface plasmon microscope," Opt. Express **19**(7), 6571–6586 (2011).

1. Introduction

In recent years there has been a growing interest in performing surface plasmon (SP) measurements within a microscopic environment [1–6]; this offers the possibility of obtaining localized high resolution measurements of local changes in refractive index as well as performing valuable imaging of cell attachment [7–9]. We have shown that the lateral resolution of SP microscopy is optimized with an interferometric arrangement and we have more recently demonstrated that similar performance can be achieved with a confocal microscope arrangement [5]. Figure 1(a) shows a conceptual diagram of SP imaging in a confocal system, as the sample is defocused there are two principal contributions to the signal arising from paths P1 and P2, which interfere with each other at the pinhole. The presence of the pinhole ensures that only radiation excited and reradiated at points '*a*' and '*b*' contribute to the SP signal so light reradiated at other points is eliminated by the pinhole. This means

#177504 - $15.00 USD Received 4 Oct 2012; revised 12 Nov 2012; accepted 19 Nov 2012; published 3 Dec 2012

that the resolution of the system is determined by the optical system rather than the propagation length of the SPs; which is the case in most SP imaging systems. As the sample is defocused interference fringes are detected in the so-called *V(z)* curve whose period depends on the angle at which the SPs are excited and reradiated, θ_p, which, in turn, is related the wave number of the SPs, $k_p = \frac{2\pi n}{\lambda}\sin\theta_p$, where λ is the wavelength of the incident light in free space and *n* is the refractive index of the couplant used in the immersion microscope objective. In order to obtain SP oscillations with a well defined period it is necessary to apodize the pupil function as otherwise the sharp edge of the aperture introduces oscillations that are unrelated to the SPs which beat with the SP oscillations. In reference [5] we used an amplitude only spatial light modulator (SLM) to apodize the illumination in the back focal plane, to ensure good quality oscillations. In the present paper we perform the same role with a phase only SLM, which also provides two other key functions: firstly it enables one to obtain a plot equivalent to the *V(z)* curve without mechanical movement, we call this *V(α)*, for reasons that will become apparent later. Furthermore, the phase SLM also allows additional processing of the signals by controlling the relative phase between paths P1 and P2 which enables one to control the signal contrast in ways not possible with an amplitude only SLM.

2. Experimental setup

The experimental system is similar to that used in [5], except that here a phase SLM (BNS 512*512 phase SLM) is used to replace the amplitude SLM; its function will be described at length in the paper.

Figure 1(b) shows a simplified schematic of the optical system. A 632.8nm He-Ne laser (10mW) was used as the illumination source and 1.45 NA oil immersion objective was used to excite SPs in air. The phase SLM was conjugate with the BFP of the immersion objective, as shown in the figure. A pellicle beam splitter was used to separate illumination and imaging paths. The light from the sample was magnified by approximately 1000 times from the sample to the CCD plane so that a point spread function occupied >100 pixels, this allowed the pinhole radius to be readily controlled by selecting different regions of camera, moreover, spreading the returning beam reduced the problem of saturating individual pixels. The CCD camera also served as a variable pinhole. Samples were mounted in the 3-dimensional (3D) scanning system, which consisted of a 3 axis mechanical stage drive, piezoelectric actuators (P621.1CD, Physik Instrumente) stage and (P-541.2CD, Physik Instrumente) giving 1 and 2 axes of movement respectively. The SLM, PZT stages and camera were controlled by software based on LABVIEW and all data were processed with MATLAB. Samples were prepared by coating gold with or without ITO on cover glasses; 2nm chromium was coated between gold and cover glass to improve the adhesion.

3. Theory of *V(z)* and *V(α)*

The output signal from a confocal microscope as a function of defocus, *z,* with a small pinhole (in practice a radius of ¼ the Airy disc diameter meets this condition) and linear input polarization into the back focal plane can be written as:

$$\begin{aligned} I(z) &= |V(z)|^2 \\ &= \left| \int_0^{2\pi} \int_0^{s_{\max}} P_{in}(s) P_{out}(s) \left[\cos^2\phi\, r_p(s) + \sin^2\phi\, r_s(s) \right] \exp(2jnkz\cos\theta)\, s\, ds\, d\phi \right|^2 \end{aligned} \quad (1)$$

Where *I(z)* is the output signal and *V(z)* is proportional to the integrated field and is thus a complex quantity. *s* is the sine of the incident angle P_{in} and P_{out} represent the input and output

#177504 - $15.00 USD Received 4 Oct 2012; revised 12 Nov 2012; accepted 19 Nov 2012; published 3 Dec 2012

pupil functions and $r_p(s)$ and $r_s(p)$ are the amplitude reflection coefficients for *p*- and *s*-polarizations respectively, θ is the angle of incidence and ϕ is the azimuthal angle.

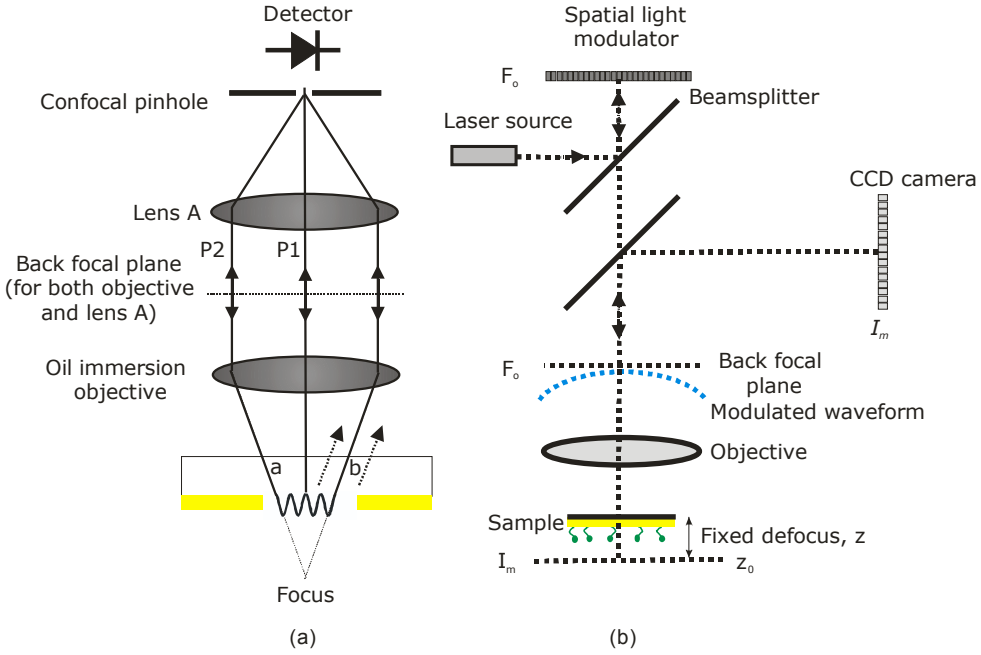

Fig. 1. (a) Simplified schematic showing operation of confocal microscope with SP excitation; (b) Schematic of optical system showing relationship between different planes in the system.

Note that positive defocus corresponds to movement of the sample away from the objective lens. $r_p(s)$ carries the information relating to the generation of the surface plasmons. As the sample is defocused towards the objective there is an interference between P1 and P2 of Fig. 1 whose periodicity is related to θ_p thus:

$$\Delta z = \frac{\lambda}{2n(1-\cos\theta_p)} \tag{2}$$

This expression is not exact because it depends on the form of the pupil function as well as variation of the modulus of the reflection coefficients, however, it is a good approximation, and more importantly from the point of view of measurement it accurately predicts small changes in periodicity as the SP propagation properties are perturbed by a small amount.

Now consider the sample at a fixed axial position, z_0, which may include $z_0 = 0$. We note that the effect of defocus is to effectively change the phase profile of the incoming beam, this means that the SLM can be used to impose the same phase distribution that would usually be imposed by a mechanical defocus. In order to replicate the effect of defocus, we project a radially varying phase distribution onto the back focal plane of the objective. The phase variation on the SLM, $\psi(s)$, is given by Eq. (3) where s again represents the sine of the incident angle which is proportional to the radial position in the back focal plane.

$$\psi(s) = \alpha\left(1-\sqrt{1-s^2}\right) = \alpha\left(1-\cos\theta\right) \tag{3}$$

gives an effective defocus

$$z_{eff} = z_0 + \frac{\alpha}{2nk} \tag{4}$$

#177504 - $15.00 USD Received 4 Oct 2012; revised 12 Nov 2012; accepted 19 Nov 2012; published 3 Dec 2012

This means that varying the curvature on the SLM by varying α moves the defocus without mechanical scanning. In effect this is equivalent to incorporating the phase shifts associated with defocus into the input pupil function. Since the light only interacts with the SLM on the incident beam path so P_{out} is unchanged.

4. Experimental results

4.1 Generating an apodized pupil function

In this subsection we consider the *V(z)* curve generated by scanning the axial defocus. In reference [5] we showed that amplitude apodization was necessary since a sharp edge to the pupil function introduces phase and amplitude fluctuations in the response which are unrelated to SP propagation. Moreover, it is also useful to attenuate light incident at angles intermediate between normal incidence and angles close θ_p as these angles do not contribute to the desired signal, so the relative amplitude of the plasmonic contribution is increased when these angles are eliminated. The angles close to normal incidence correspond to path P1 and those at higher angles correspond to path P2 of Fig. 1(a).

In our previous publication [5] we used binary modulation to generate desired amplitude of the pupil function by changing the density of 'on' and 'off' pixels in direct proportion to the required strength of the pupil function in the measurement region. This was performed using a random number generator and selecting an on pixel with probability proportional to the local amplitude. Since we are restricted here to using a phase only modulator we simply used a 2 by 2 block of pixels as a 'super pixel' and selected these units in the same way as done previously where an 'on' group of pixels would be in phase, whereas and 'off' pair would have two pixels in phase and two in antiphase (many other possibilities are also possible). We chose to use a 2 by 2 block rather than a pair of pixels simply to maintain the symmetrical shape along two axes. In addition to modulating the amplitude this procedure also allows one to impose a local phase since the pixels constituting an 'on' pixel only need to be in phase and their actual phase can be controlled independently. This point is crucial in the sections that follow. Figure 2(c) shows *V(z)* curves obtained with different pupil functions, where we see that the hard edged pupil (green) has a less well defined period and the defocus is greater than 3 microns before the ripples due to the SPs dominate; this compares to about 2 microns for the other cases.

#177504 - $15.00 USD Received 4 Oct 2012; revised 12 Nov 2012; accepted 19 Nov 2012; published 3 Dec 2012

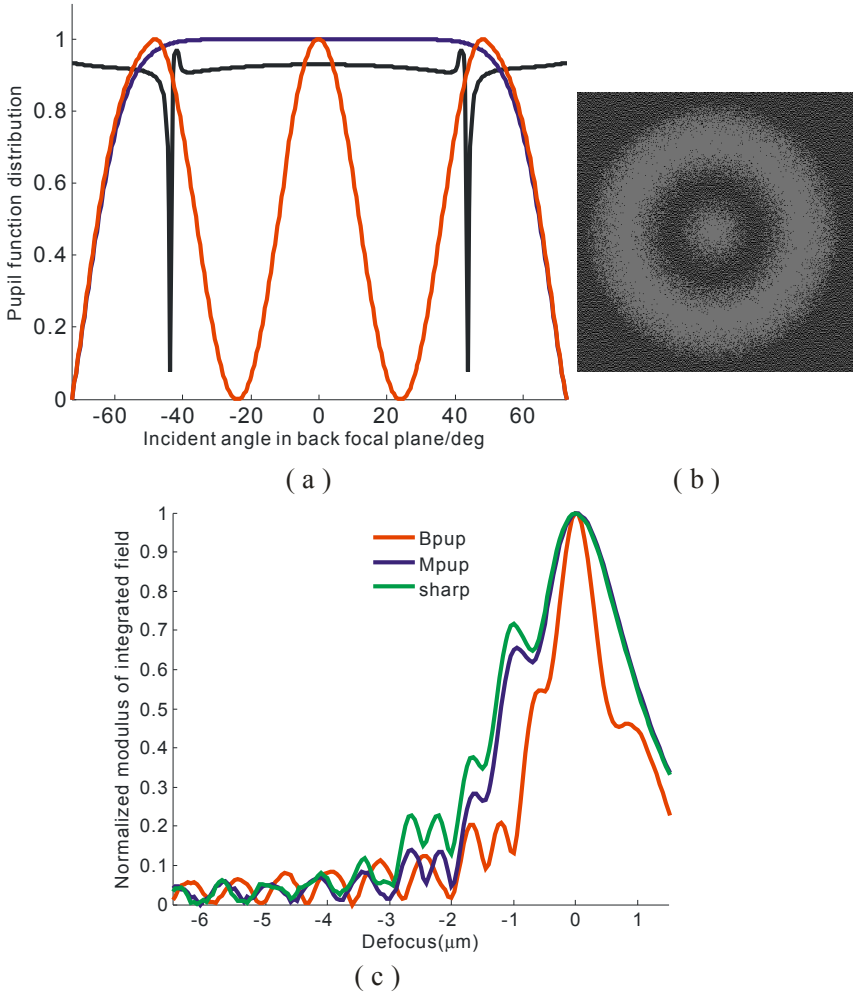

Fig. 2. (a) Pupil function distribution (red curve and blue curve are the pupil functions used in the experiment, the black curve show the calculated reflection coefficient for *p*-incident polarization on an uncoated sample. Note the blue curve overlaps the red for large incident angles (b) is the 2D pattern on the SLM used to produce the red curve, the random variations are explained in the text; (c) *V(z)* curves obtained using different pupil functions (green curve was produced by a pupil function which was constant over the whole aperture, the red and blue curves correspond to the pupils of the same color in (a).

4.2 V(α) curves: defocusing without scanning

Figure 3 shows a comparison between a *V(z)* curve and a *V(α)* curve taken on the same sample. The values of α have been obtained from the phase profile on the SLM using Eq. (3). No mechanical scanning was used to obtain the *V(α)* curves. We note in both curves that there is region of rapid oscillation equivalent to a defocus between approximately –1 and –2 microns this is due to aberration in the objective possibly due to some surface damage, however, beyond –2 microns there is a clear oscillation due to the presence of the SPs which show equivalent behaviour and predict a value of θ_p = 43.5 degrees. Figure 3(b) upper subfigure shows the phase distributions imposed corresponding to defocuses of –4 and –0 microns respectively. The corresponding phase values were much greater than 2π and

#177504 - $15.00 USD Received 4 Oct 2012; revised 12 Nov 2012; accepted 19 Nov 2012; published 3 Dec 2012

therefore needed to be wrapped. Figure 3(b) lower subfigure shows the wrapped phase distribution corresponding to a defocus of –4 microns.

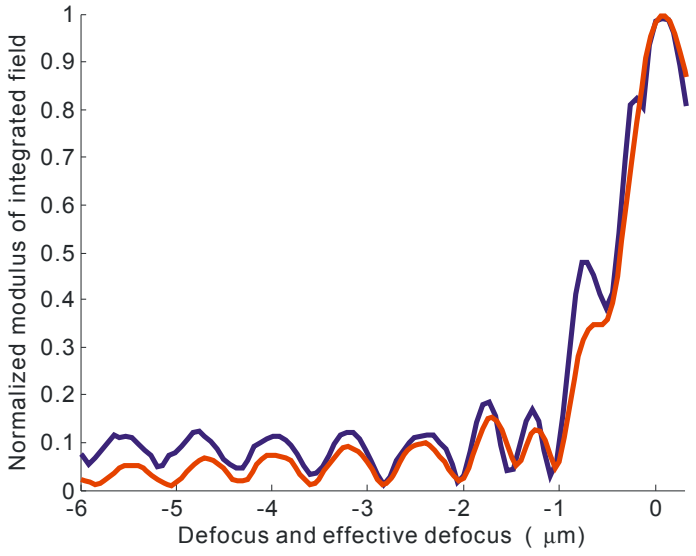

(a)

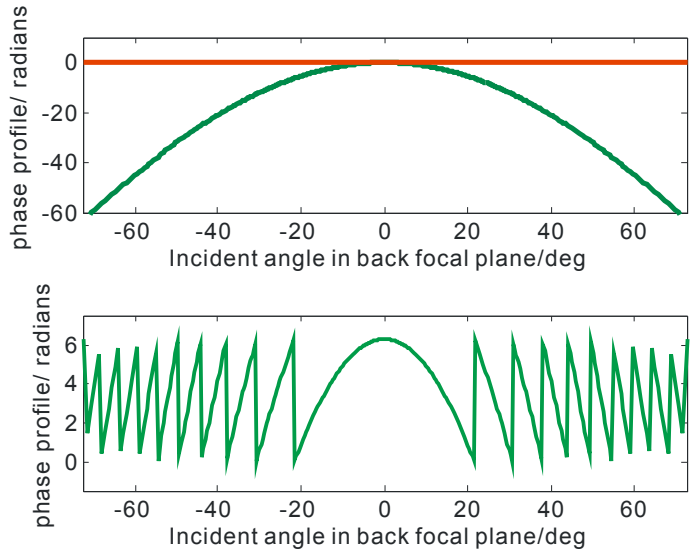

(b)

Fig. 3. Comparison between *V(z)* and *V* (z_{eff}), the red line refers to the real *V(z)* curve and blue line refers to the effective *V(z)* calculated from *V(α)* (b) Upper subfigure shows the phase distributions imposed corresponding to defocuses of –4 (green curve) and 0 (red line) microns respectively. Lower subfigure shows the wrapped phase distribution corresponding to a defocus of –4 microns. For positive defocus the curves are inverted

Figure 4 shows a comparison between $V(z_{eff})$ curves obtained on a gold sample and gold layer coated with a thin layer of ITO, we can see that ripples associated with the coated region have a shorter period compared to the uncoated region (0.714 μm compared to 0.739 μm),

#177504 - $15.00 USD Received 4 Oct 2012; revised 12 Nov 2012; accepted 19 Nov 2012; published 3 Dec 2012

corresponding plasmon angles of 44.93° and 43.48° respectively. The difference in θ_p obtained between the coated and uncoated region is attributed to layer of ITO of thickness 7.8 nm, which is close to the value set in the deposition process.

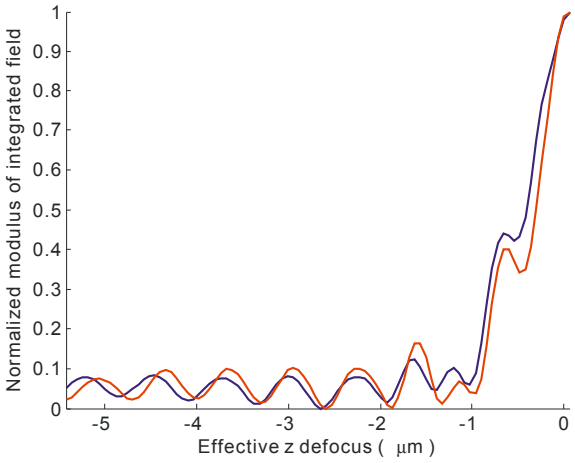

(a)

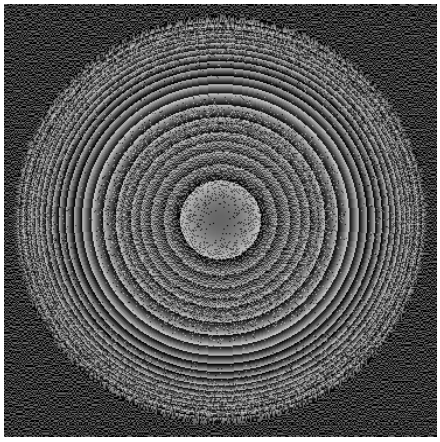

(b)

Fig. 4. (a) $V(\alpha)$ comparison between uncoated and ITO coated sample, the red line is the ITO coated case and blue line is the uncoated case; (b) is one wrapped pattern used in the experiment. The physical defocus, z_0, was set to zero, that is the sample was in focus.

4.3 Changing the offset defocus

Equation (3) shows that the effects of the physical defocus and defocus imposed by the SLM are additive. This effect is borne out in Fig. 5 which shows how the curves are displaced as the physical defocus is changed. For instance, in the case of the green curve there is a physical defocus of −2 microns so an equal and opposite effective defocus from the SLM is required. The interesting feature is that although the periodicity of the ripples is essentially unchanged the quality of curves is actually better when the physical defocus is small. This is somewhat counterintuitive since large defocuses mean the additional curvature imposed by the SLM is small. Preliminary experiments and simulations show that when large physical

#177504 - $15.00 USD Received 4 Oct 2012; revised 12 Nov 2012; accepted 19 Nov 2012; published 3 Dec 2012

defocuses are imposed the effect of small misalignments between the axis of the two defocus mechanisms (physical and SLM) introduce strong aberrations which degrade the $V(\alpha)$ curve. Moreover, with two defocus mechanisms the system appears very sensitive to sample tilt. Since the quality of the oscillations is not noticeably degraded (see Fig. 4(b)) when there are large numbers of phase wraps on the SLM pattern our experiments were performed with little or no physical defocus.

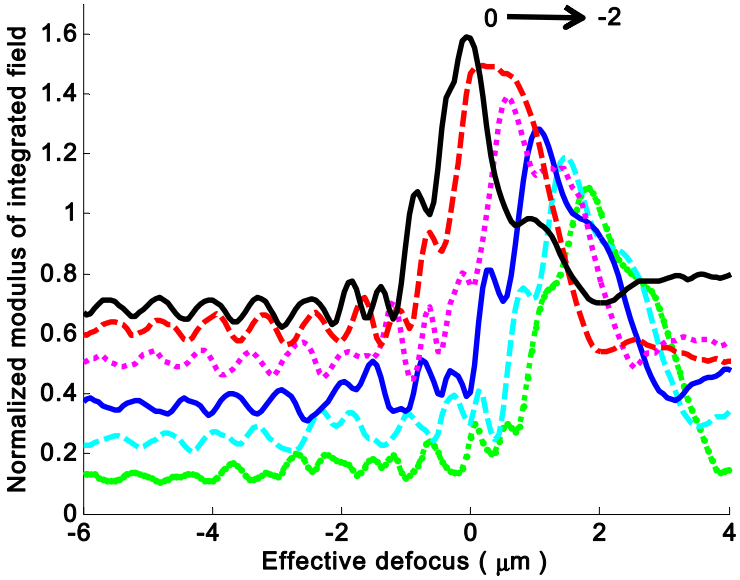

Fig. 5. $V(\alpha)$ curves obtained with different amounts of physical defocus . The black line to the bottom green line, represent fixed physical defocuses of 0, –0.4, –0.8, –1.2, –1.6, –2 respectively. The curves are displaced along the y-axis by 0.2 units for clarity. Line order black (solid), red(dashed), magenta (dotted), blue (solid), cyan (dash), green (dotted).

4.4 Additional phase shifting of the reference beam

Since the phase SLM performs all the functions necessary in the signal processing we can simply modify the expression for $\psi(s)$ so that we add an additional phase shift, β, below incident angles corresponding to $\sin^{-1}(s_1)$.

$$\psi(s)=\begin{cases}\alpha\left(1-\sqrt{1-s^2}\right)+\beta, \text{for } s<s_1\\ \alpha\left(1-\sqrt{1-s^2}\right), \text{for } s\geq s_1\end{cases} \tag{5}$$

so that we simply add an additional phase shift for incident angles below sin-1(s1) . Where s1 defines the sine of incident angle in which an additional phase shift is imposed. At a given defocus this changes the relative phase between paths P1 and P2 in Fig. 1. Figure 6 shows this effect very clearly where the period of the ripple is unchanged but with an additional phase shift imposed. This provides an additional means of changing contrast in SP imaging, for instance, displacing the curves to the position where the gradients change most rapidly will enhance contrast, whereas a 180 deg. phase shift will reverse contrast.

#177504 - $15.00 USD Received 4 Oct 2012; revised 12 Nov 2012; accepted 19 Nov 2012; published 3 Dec 2012

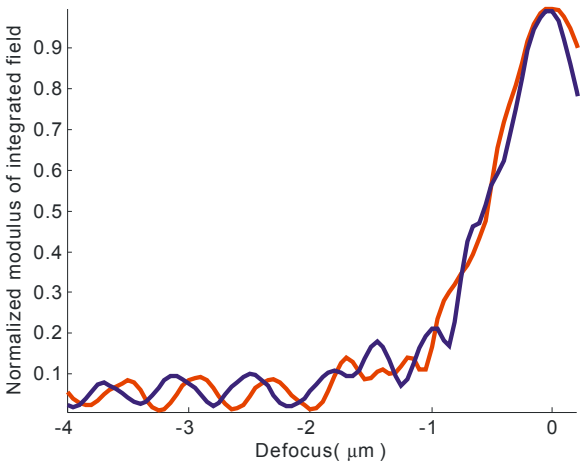

(a)

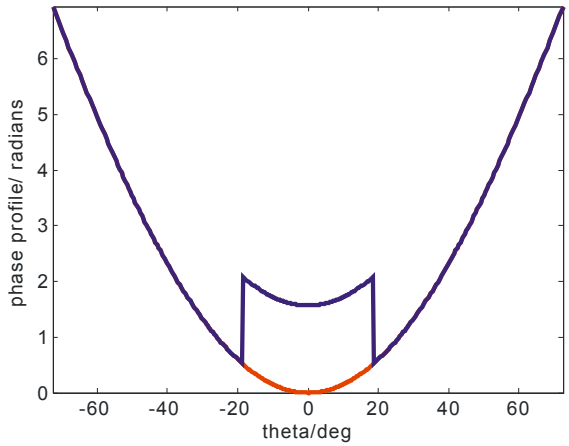

(b)

Fig. 6. (a) *V(α)* curves obtained with two different phase shifts of the reference, red curve refers to the non-phase shifting case and the blue line refers to the case where a shift of 90° on the reference beam is applied; (b) a phase profile pattern, the red curve is the original phase profile and blue curve refers to reference bean phase shifting of $\frac{\pi}{2}$, above 20° incident angle the two curves are identical.

4.5 Misalignment of the phase SLM

Figure 7 shows the effect of moving the phase SLM from the optimal position. We can see that the period of the ripples does not change significantly but even a very small displacement of 1% of the radius of the aperture in the back focal plane degrades the number of observable ripples dramatically, clearly this phase error is exacerbated for large curvatures. When the SLM is displaced by 2% of the aperture radius the interference between reference and SPs is barely visible at any defocus.

#177504 - $15.00 USD Received 4 Oct 2012; revised 12 Nov 2012; accepted 19 Nov 2012; published 3 Dec 2012

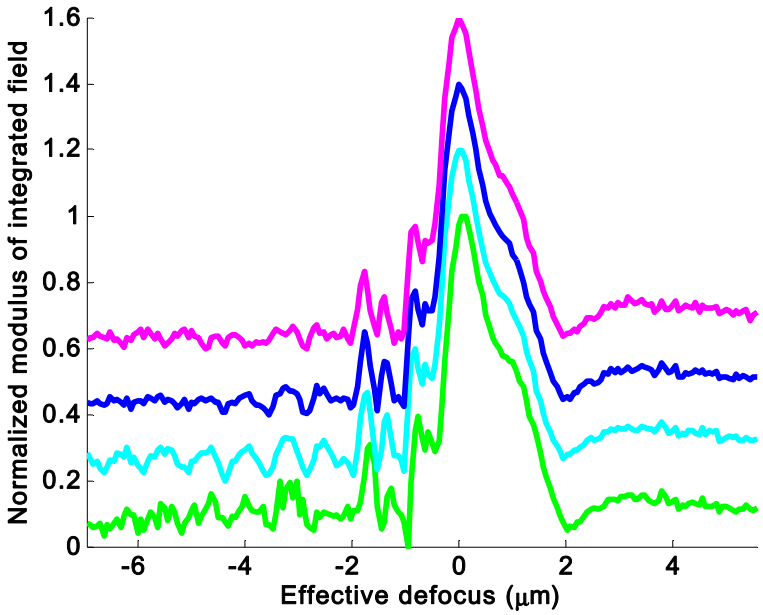

Fig. 7. The effect of SLM misalignment on the quality of the $V(\alpha)$ curves. The SLM was misaligned by –0.01, 0, 0.01, 0.02 units of the back focal plane aperture from the lower green line to the upper magenta line. The curves are displaced along the y-axis by 0.2 units for clarity.

5. Conclusion

This paper has shown how a phase SLM can greatly extend the utility of confocal based SP sensing and imaging. A crucial feature in SP imaging is that contrast changes and quantification of the SP k-vector can be obtained by axially scanning of the sample. The present paper shows that this may be achieved functionally by simply altering the phase profile of the SLM. This removes the need for precision mechanical components and is inherently more stable and also potentially quicker.

We also show preliminary results that demonstrate that further processing of the response may be obtained by changing the phase between the reference beam (P1 in Fig. 1) and the SP beam (P2 in Fig. 1), this provides an additional contrast mechanism. We also plan to investigate whether phase stepping can be used to extract the SP phasor independently of the reference phasor thus performing a direct measurement of SP decay.

Future work will extend the ideas discussed here to imaging in aqueous media and we also intend to show that the pixellated detector of the SLM can be used to extract more information with better signal to noise than a simple variable sized pinhole.

Acknowledgments

The authors gratefully acknowledge the financial support of the Engineering and Physical Sciences Research Council (EPSRC) for a platform grant, ‘Strategies for Biological Imaging’, the UK and China Scholarship Council (CSC) for Bei Zhang’s Scholarship. We thank Dr. Jing Zhang for Bei Zhang’s guidance in optical imaging and Dr. Kevin Webb for his practical insights.

#177504 - $15.00 USD Received 4 Oct 2012; revised 12 Nov 2012; accepted 19 Nov 2012; published 3 Dec 2012